Three-dimensional vortex configurations in a rotating Bose-Einstein condensate

Amandine Aftalion* and Ionut Danaila†
Laboratoire Jacques-Louis Lions, Université Paris 6, 175 rue du Chevaleret, 75013 Paris, France
(Received 17 March 2003; published 11 August 2003)

We consider a rotating Bose-Einstein condensate in a harmonic trap and investigate numerically the behavior of the wave function which solves the Gross-Pitaevskii equation. Following recent experiments [P. Rosenbuch, V. Bretin, and J. Dalibard, Phys. Rev. Lett. **89**, 200403 (2002)], we study in detail the line of a single quantized vortex, which has a U or S shape. We find that a single vortex can lie only in the x-z or y-z plane. S-type vortices exist for all values of the angular velocity Ω while U vortices exist for Ω sufficiently large. We compute the energy of the various configurations with several vortices and study the three-dimensional structure of vortices.

DOI: 10.1103/PhysRevA.68.023603 PACS number(s): 03.75.Kk, 02.70.−c

I. INTRODUCTION

Several experimental groups have produced vortices in Bose-Einstein condensates (BECs) [1–6]. One type of experiments consists in imposing a laser beam on the magnetic trap holding the atoms to create a harmonic anisotropic rotating potential. For a prolate trap, it has been observed [2,3,6] that when a single vortex exists, the vortex line is not straight along the axis of rotation, but bending. Theoretical works [7,8] establish a simpler expression of the Gross-Pitaevskii energy that only depends on the vortex lines. In Ref. [8], it is proved that bending occurs for prolate condensates, but not for oblate ones.

Minimization algorithms [9,10] have been used to compute local minima of the Gross-Pitaevskii energy and provide an evidence of the bending in the same setting as in the experiments. Bending (or U) vortices are described in detail and multiple-vortex configurations are addressed in these studies.

Recently, authors of Ref. [6] have further studied configurations with a single-vortex line. They have observed planar bent vortices U but also different configurations S. They study the length of the line, its deviation from the center, and its angular momentum.

In this paper, motivated by the recent experiments by Rosenbuch *et al.* [6], we compute local minimizers of the Gross-Pitaevskii energy and want to understand the various vortex configurations observed in the experimental setting: U vortices but also S vortices. We look for solutions with up to four vortices and describe their three-dimensional (3D) structure. Different solution branches are followed and the evolution of the corresponding energy and angular momentum are shown. The framework of this study is the case of a prolate condensate where bending is an important phenomenon.

We consider a pure BEC of N atoms confined in a harmonic trapping potential rotating along the z axis at angular velocity Ω. The equilibrium of the system corresponds to local minima of the Gross-Pitaevskii energy in the rotating frame

$$\mathcal{E}(\phi)=\int_{\mathcal{D}}\frac{\hbar^2}{2m}|\nabla\phi|^2+\hbar\mathbf{\Omega}\cdot(i\phi,\nabla\phi\times\mathbf{x})+\frac{m}{2}\omega_x^2(x^2+\alpha^2y^2+\beta^2z^2)|\phi|^2+Ng_{3\mathrm{D}}|\phi|^4, \quad (1)$$

where $g_{3\mathrm{D}}=4\pi\hbar^2a/m$ and the wave function ϕ is normalized to unity $\int_{\mathcal{D}}|\phi|^2=1$.

For numerical purposes, it is convenient to rescale the variables as follows: $\mathbf{r}=\mathbf{x}/R$, $u(\mathbf{r})=R^{3/2}\phi(\mathbf{x})$, where $R=d/\sqrt{\varepsilon}$ and

$$d=\left(\frac{\hbar}{m\omega_x}\right)^{1/2},\quad \varepsilon=\left(\frac{d}{8\pi Na}\right)^{2/5},\quad \tilde{\Omega}=\Omega/(\varepsilon\omega_x). \quad (2)$$

In this scaling, the Thomas-Fermi limit of u is

$$\rho_{\mathrm{TF}}(\mathbf{r})=\rho_0-(x^2+\alpha^2y^2+\beta^2z^2). \quad (3)$$

Then, we use the dimensionless energy introduced in Ref. [7]

$$E(u)=H(u)-\tilde{\Omega}L_z(u), \quad (4)$$

with

$$H(u)=\int_{\mathcal{D}}\frac{1}{2}|\nabla u|^2-\frac{1}{2\varepsilon^2}\rho_{\mathrm{TF}}|u|^2+\frac{1}{4\varepsilon^2}|u|^4, \quad (5)$$

$$L_z(u)=i\int_{\mathcal{D}}\bar{u}\left(y\frac{\partial u}{\partial x}-x\frac{\partial u}{\partial y}\right), \quad (6)$$

defined in the domain $\mathcal{D}=\{\rho_{\mathrm{TF}}(\mathbf{r})\geqslant 0\}$.

A. Numerical method

We compute critical points of $E(u)$ by solving the norm-preserving imaginary time propagation of the corresponding equation:

$$\frac{\partial u}{\partial t}-\frac{1}{2}\nabla^2u+i(\tilde{\mathbf{\Omega}}\times\mathbf{r})\cdot\nabla u=\frac{1}{2\varepsilon^2}u(\rho_{\mathrm{TF}}-|u|^2)+\mu_\varepsilon u, \quad (7)$$

*Electronic address: aftalion@ann.jussieu.fr
†Electronic address: danaila@ann.jussieu.fr

with $u=0$ on $\partial\mathcal{D}$ and μ_ε the Lagrange multiplier for the constraint $\int_{\mathcal{D}}|u|^2=1$. A hybrid three steps Runge-Kutta-Crank-Nicolson scheme [11] is used to march in time (Δt is the time step):

$$\frac{u_{l+1}-u_l}{\Delta t}=a_l\mathcal{H}_l+b_l\mathcal{H}_{l-1}+c_l\nabla^2\left(\frac{u_{l+1}+u_l}{2}\right), \tag{8}$$

where $\mathcal{H}$ contains the terms with explicit time discretization:

$$\mathcal{H}(u)=\frac{1}{2\varepsilon^2}u(\rho_{\mathrm{TF}}-|u|^2)+\mu_\varepsilon u-i(\tilde{\mathbf{\Omega}}\times\mathbf{r})\cdot\nabla u. \tag{9}$$

The corresponding constants for every step ($l=1,2,3$) are

$$\begin{gathered} a_1=8/15,\quad a_2=5/12,\quad a_3=3/4,\\ b_1=0,\quad b_2=-17/60,\quad b_3=-5/12,\\ c_1=8/15,\quad c_2=2/15,\quad c_3=1/3. \end{gathered} \tag{10}$$

The resulting semi-implicit scheme is second-order time accurate and allows reasonably large time steps, making it appropriate for long-time integration. The large sparse matrix linear systems resulting from the implicit terms are solved by an alternating direction implicit factorization technique.

For the spatial discretization, we use finite differences on a Cartesian uniform mesh with periodic boundary conditions in all directions. To accurately resolve sharp gradients of the variable in the presence of vortices, low numerical dissipation and very accurate schemes are required for the spatial derivatives. A sixth-order compact finite difference scheme [12] with spectral-like resolution is chosen to this end.

B. Physical and numerical parameters

The values of the constants in Eq. (7) are set to $\varepsilon=0.02$, $\alpha=1.06$, $\beta=0.067$, corresponding to the experiments of Refs. [3,10] ($m=1.445\times10^{-26}$ kg, $a=5.8\times10^{-11}$ m, $N=1.4\times10^5$, and $\omega_x=1094$ s^{-1}). The angular frequency Ω will be varied from 0 to the maximum value of $0.9\omega_x$, for which no deformation of the condensate has to be taken into account.

Equation (7) is propagated in imaginary time until the evolution of energy (4) has a gradient in time smaller than 10^{-6}. The numerical domain is fixed to an elongated box $(x,y,z)\in[-0.6,0.6]\times[-0.6,0.6]\times[-8.5,8.5]$. A refined grid with $72\times72\times510$ nodes is used, which is sufficient to achieve grid independence.

Different initial conditions are used in order to trigger single- or multiple-vortex configurations and follow the corresponding branches as Ω is varied. The simplest initial condition assumes a steady-state solution $u(x,y,z)=\sqrt{\rho_{\mathrm{TF}}(x,y,z)}$. It is useful to study vortex-free configurations and their degeneracy into multiple-vortex configurations when increasing the value of Ω. Initial conditions with vortices are obtained by superimposing to the steady state a simple ansatz for the vortex. For example, an initial condition with a centered straight vortex of radius ε is obtained by imposing

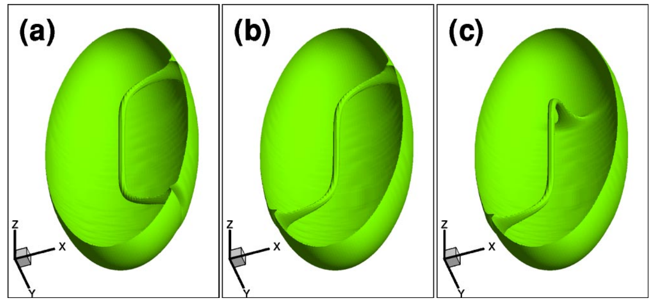

FIG. 1. Single-vortex configurations in BECs: (a) U vortex, (b) planar S vortex, (c) nonplanar S vortex. Isosurfaces of lowest density within the condensate.

$$u(x,y,z)=\sqrt{\rho_{\mathrm{TF}}}\,u_\varepsilon, \tag{11}$$

$$u_\varepsilon=\sqrt{0.5\left\{1+\tanh\left[\frac{4}{\varepsilon}(r-\varepsilon)\right]\right\}}\exp(i\varphi),$$

where (r,φ) are the polar coordinates in the (x,y) plane. The 3D shape of the vortex can be easily modified by shifting the center r_0 of the vortex in successive (x,y) planes; for instance, to obtain a planar S shape vortex, the following function can be used:

$$r_0(z)=\begin{cases} -1+\tanh\left[\alpha_v\left(1+\dfrac{z}{\beta_v}\right)\right]\Big/\tanh(\alpha_v), & z<0\\ 1+\tanh\left[\alpha_v\left(-1+\dfrac{z}{\beta_v}\right)\right]\Big/\tanh(\alpha_v), & z\geqslant 0. \end{cases} \tag{12}$$

The constants α_v,β_v control, respectively, the curvature and the height of the vortex.

We first focus on single-vortex configurations and describe later multivortex configurations.

II. SINGLE-VORTEX LINES

We have observed three different types of single-vortex configurations as shown in Fig. 1: planar U vortices, planar S vortices, and nonplanar S vortices. The U vortices are the bent vortices computed in Refs. [9,10] and theoretically studied in Refs. [7,8]. They are global minimizers of the energy. The S configurations were observed experimentally very recently [6] and are only local minimizers of the energy.

A. *U* vortex

The U vortex is a planar vortex formed of two parts: the central part is a line which stays on the z axis and the outer part reaches the boundary of the condensate perpendicularly. When Ω increases, the central straight part gets longer (Fig. 2) and the angular momentum L_z increases to 1 (Fig. 3).

The U vortex is obtained by starting with an initial condition containing a straight vortex away from the z axis. In fact, the U vortex lies either in the x-z or y-z plane. Starting with an initial condition that is not in one of these planes

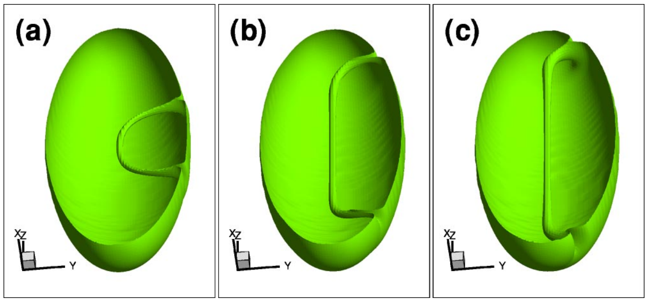

FIG. 2. Single U vortex configurations for $\Omega/\omega_x = 0.42$ (a), 0.58 (b), 0.78 (c).

yields a final state in the y-z plane, which is the plane closest to the z axis.

The shape of the the U vortex and its preferred location in the y-z plane can be analyzed using the approximate energy derived in Refs. [7,8]: setting the vortex-free solution to zero energy, then the energy of a vortex line γ can be approximated by

$$\mathcal{E}_\gamma = \int_\gamma \rho_{\mathrm{TF}}\, dl - C\Omega \int_\gamma \rho_{\mathrm{TF}}^2\, dz, \tag{13}$$

where the first term is the limit of the energy H and the second term is $-\Omega L_z$. Here, C is a constant which depends on the experimental parameters and ρ_{TF} is given by Eq. (3). If γ is not in the x-z or y-z plane, then one can construct small perturbations of γ that preserve ρ_{TF} and lower the energy. This implies that γ cannot be a critical point of the energy because the gradient is not zero. Of course, if the ellipticity of the cross section is small, the gradient is small, which may allow to observe these configurations.

In order to understand the existence of the straight central part of the U vortex, one can also refer to the analysis of Ref. [8]: from Eq. (13), we can infer that a vortex line with a lower energy than the vortex-free solution is obtained when the quantity $\rho_{\mathrm{TF}} - C\Omega\rho_{\mathrm{TF}}^2$ is negative, i.e., $C\Omega\rho_{\mathrm{TF}} > 1$. Let $\bar{\Omega}$ be such that $C\bar{\Omega}\rho_0 = 1$; it corresponds to the 2D critical velocity for the existence of a vortex in the plane $z=0$. For Ω close to $\bar{\Omega}$, the inner region where $C\Omega\rho_{\mathrm{TF}} > 1$ is concentrated near the center of the condensate. In this region, the vortex line has to be straight (see Ref. [8]). This straight part is getting longer as Ω increases since the region where $C\Omega\rho_{\mathrm{TF}} > 1$ is getting bigger. This region corresponds to $\Omega > \Omega_{2D}(z)$, where $\Omega_{2D}(z)$ is the critical velocity for the existence of a vortex in the two-dimensional section where z is constant. In the outer region, the vortex reaches the boundary using the shortest path.

Figure 3 shows the energy and angular-momentum variation with Ω for the single-vortex configurations. The U vortices exist only for Ω bigger than a critical value $\Omega_c = 0.42\omega_x$. It is interesting to note that at Ω_c, the energy of the U vortex is bigger than the energy of the vortex-free solution (we have set to zero the energy of the vortex-free solution). A zoom in this region shows that Ω_c is very close to the angular velocity Ω_1 for which the energy of the vortex-free solution is equal to the energy of the U vortex.

Figure 3 also shows that the angular momentum L_z of the U vortex for $\Omega = \Omega_c$ does not go to 0. This suggests that in fact there could be another U solution for $\Omega > \Omega_c$. Using an ansatz, another type of U solution is obtained in Ref. [10] which is a saddle point of the energy: it is away from the axis and has a lower angular momentum. In Ref. [8], it is proved rigorously that for small Ω, there is no U as a critical point of the energy.

For an initial condition with a straight vortex centered on the z axis, if $\Omega < 0.8\omega_x$, the straight vortex is unstable and the final configuration is a U, but if $\Omega > 0.8\omega_x$, the straight vortex is stable. This is in agreement with the result of Ref. [8] where the local stability of the straight vortex for larger Ω is proved.

For small Ω, the U vortex disappears and a vortex-free configuration is obtained, while for larger Ω, the U vortex degenerates into a three-vortex configuration (described later).

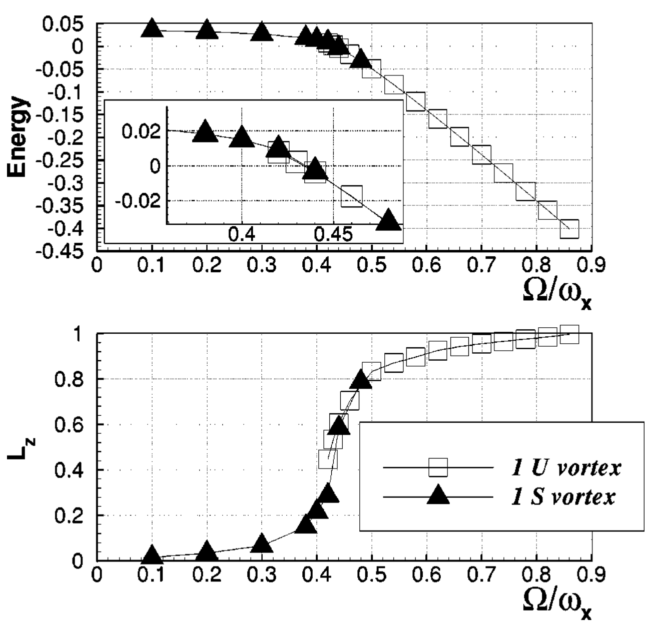

FIG. 3. Energy (in units of $\hbar\omega_x$) and angular momentum per particle (in units of $\hbar$) for the single-vortex configurations.

B. S vortex

Motivated by the experiments of Ref. [6], we compute new critical points of the energy, which are S configurations (see Fig. 1). Several numerical experiments were performed, starting from different initial conditions containing an ansatz for the S vortex (see Sec. I B).

The planar S can be regarded as a U, with the half part in the plane $z<0$ rotated with respect to the z axis by 180° (see Fig. 4). The nonplanar S are such that the projections of the branches on the x-y plane are orthogonal, i.e., the rotation of the branches is of 90°. We could check that nonplanar S configurations with an angle between the branches different from 90° do not exist.

As already mentioned for the U vortex, stable planar S configurations lie either in the x-z or y-z plane. As for the U,

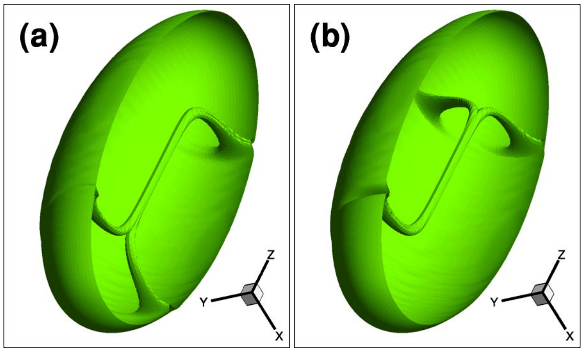

FIG. 4. Comparison between the single-vortex configurations obtained for the same angular velocity $\Omega/\omega_x = 0.44$. Superposition of the U and S vortex (a) and the planar and nonplanar S vortex (b).

this can be explained using the limiting energy obtained in Ref. [8] and considering separately the upper or lower part of the S. As soon as the cross section is not a disc, if the upper or lower branch of the S configuration does not lie in the x-z or y-z plane, then the gradient of the vortex line energy (13) can never be zero when γ is varied.

The S vortices exist for all values of Ω while the U exist only for $\Omega > \Omega_c$. When Ω decreases, the extension of the S along the z axis goes downwards as shown in Fig. 5, the angular momentum decreases to zero (Fig. 3) and the vortex tends to the horizontal axis. Note that a vortex along the horizontal axis has $L_z = 0$, but a positive energy. On the other side, when Ω increases, the S gets straighter and it tends to the vertical axis.

The global minimum of the energy is never an S. But the difference in energy (and angular momentum) between U and S vortices is very small, as illustrated in Fig. 3 because an S vortex is almost like a U with a half part rotated by 180°.

C. Minimizer with fixed L

As pointed out in Ref. [6], the minimization problem that is related to the experiments, is rather to minimize H [see Eq. (5) while fixing L_z, rather than minimizing $E = H - \Omega L_z$. This has been studied in the two-dimensional setting in Ref. [13]. One can notice that if a given configuration with $H = h$ and $L_z = l$ minimizes $E = H - \Omega L_z$ for some Ω, then h minimizes H under the constraint that $L_z = l$: indeed if $H' = H(u)$ with $L_z(u) = l$, then $H' - \Omega l \geqslant h - \Omega l$, since (h,l) minimizes E, and this implies that $H' \geqslant h$. Moreover, Ω is the slope of the curve $H(L_z)$ at the point (h,l) and the property of minimizing E, that is, for all h', l',

$$h' - \Omega l' \geqslant h - \Omega l, \tag{14}$$

implies that the curve $H(L_z)$ lies above its tangent at this point.

We have plotted H as a function of L_z (Fig. 6). We can check that the curve is convex, and above its tangent, which is consistent with the fact that we have computed minimizers of the energy.

We know that the U solution exists for $\Omega \geqslant \Omega_c$ and has $L_z > 0.4$. For $L_z < 0.4$, we expect that the process of minimizing H with fixed L_z would produce U vortices and the curve $H(L_z)$ should be concave in this region. In Ref. [8], we have proved that for L_z close to 0, $H \geqslant C L_z^{2/3}$, which is a first indication to the concavity of the curve.

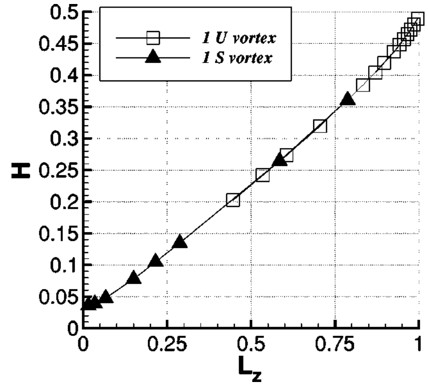

FIG. 6. H vs L_z for single-vortex configuration.

III. MULTIPLE VORTICES

Multiple-vortex configurations are obtained based upon different numerical strategies. The first one is to start the computation from a vortex-free steady state and to abruptly increase Ω to a very high value; multiple vortices are thus obtained. The second strategy is to generate an initial condition with vortices as described in Sec. I B (the advantage being the control of the shape and initial arrangement of the vortices).

Both techniques are used to follow solution branches with

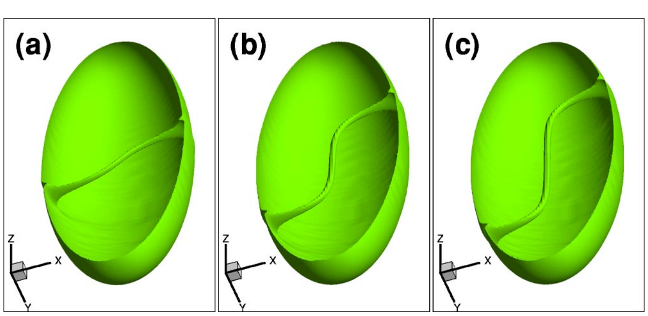

FIG. 5. Single S vortex configuration for $\Omega/\omega_x = 0.38$ (a), 0.44 (b), 0.48 (c).

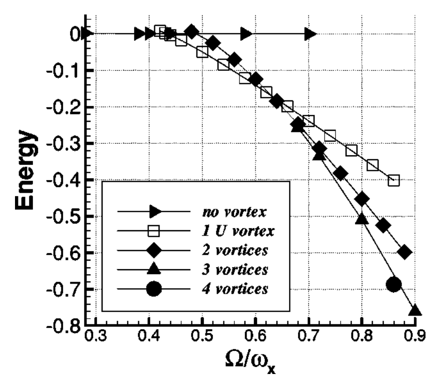

FIG. 7. Energy (in units of $\hbar\omega_x$) for all studied configurations.

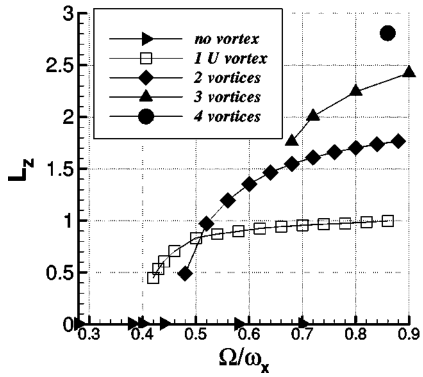

FIG. 8. Angular momentum L_z (in units of $\hbar$) for all studied configurations.

two, three, or four vortices in the condensate. Figures 7 and 8 display energy and angular momentum vs Ω for all studied configurations.

A. Three vortices

When Ω is increased, the single *U* vortex solution switches to a three-vortex configuration ($\Omega=0.9\omega_x$). As shown in Fig. 9(a), the configuration is invariant under rotation in a central plane near $z=0$ but not near the edges. For large Ω, three-dimensional views show [Figs. 9(a) and 9(b)] that there are two vortices of similar size and a longer one which is bending near the boundary. For $\Omega=0.8\omega_x$, all vortices display contorted shapes [Fig. 9(c)], very similar to those reported in Ref. [9]. Let us point out that the angular momentum of all these three-vortex configurations is lower than 3 (see Fig. 8).

When we put as an initial condition a configuration with three identical *U* vortices at 120°, in the final state, one of them gets a little longer [Fig. 10(a)] and the symmetry is lost. This configuration has almost the same energy and angular momentum as the configuration displayed in Fig. 9(b). Conversely, for the initial condition with three straight vortices

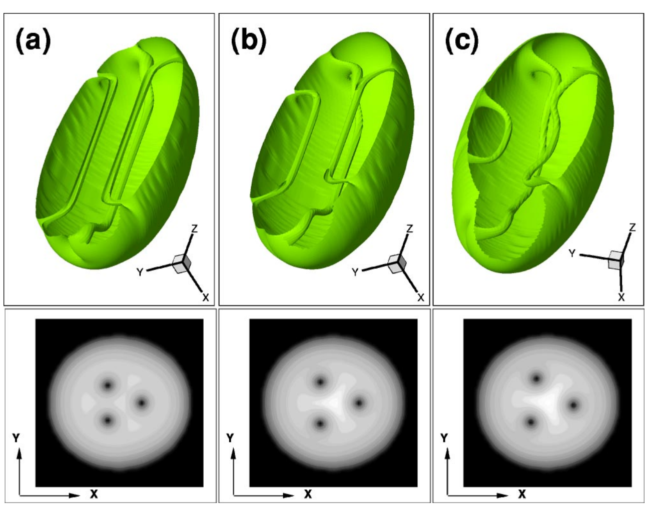

FIG. 9. Three-vortex configuration for $\Omega/\omega_x=0.9$ (a), 0.72 (b), 0.68 (c). Lower pictures show isocontours of $|u|$ in the central $z=0$ cut plane.

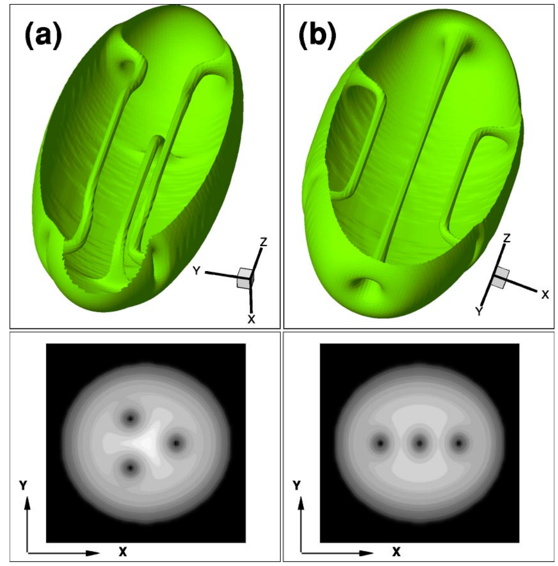

FIG. 10. Three-vortex configuration obtained for the same $\Omega/\omega_x=0.72$, from different initial conditions: three identical *U* vortices at 120° (a) and three straight vortices in a row on the *x* axis (b). Lower pictures show isocontours of $|u|$ in the central $z=0$ cut plane.

on the *x* axis, the symmetry is preserved [Fig. 10(b)], but it has a higher energy than the previous one.

When Ω further decreases, the three-vortex branch switches to a two vortex displaying irregular shapes (Fig. 11).

B. Two vortices

The two-vortex branch presented in this section is obtained by starting from a vortex-free solution and suddenly increasing Ω to a value of $0.8\omega_x$. The configuration is planar and symmetric, such as twice a single *U* vortex, but away from the axis (there is a repulsion between the lines).

When Ω increases, the lines are almost straight and get closer to each other. This is in agreement with the fact that when Ω gets large, the straight vortex is a local minimizer of the energy. Hence, the bending is no longer the important phenomenon (Fig. 12).

We recall that decreasing Ω from a configuration with three vortices, we obtain two vortices that are not symmetric,

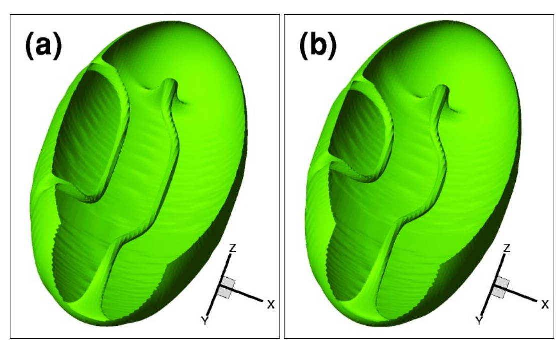

FIG. 11. Two vortices obtained from the three-vortex configuration when the value of Ω/ω_x is decreased to 0.64 (a) and 0.6 (b).

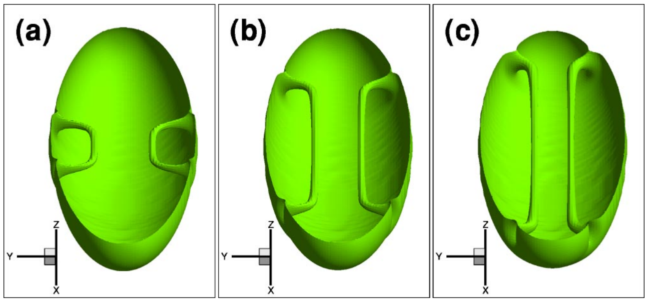

FIG. 12. Configuration with two symmetric vortices for $\Omega/\omega_x = 0.48$ (a), 0.6, (b) 0.8 (c).

one being longer than the other (Fig. 11). This configuration has a slightly higher energy than the two symmetric vortices.

C. Four vortices

Starting from an initial condition without vortices and increasing Ω to $0.86\omega_x$, we have obtained stable configurations with four curved vortices [Fig. 13(a)]. When Ω decreases, this configuration rapidly degenerates into a three-vortex state. For lower Ω, we could obtain stable configurations with four symmetric vortices [Fig. 13(b)], but with higher energy. The location of the vortices in the plane $z=0$ is the same.

We have to point out that for the initial condition of four identical vortices, the symmetry is preserved as displayed in Fig. 13(b), which is not the case for three vortices.

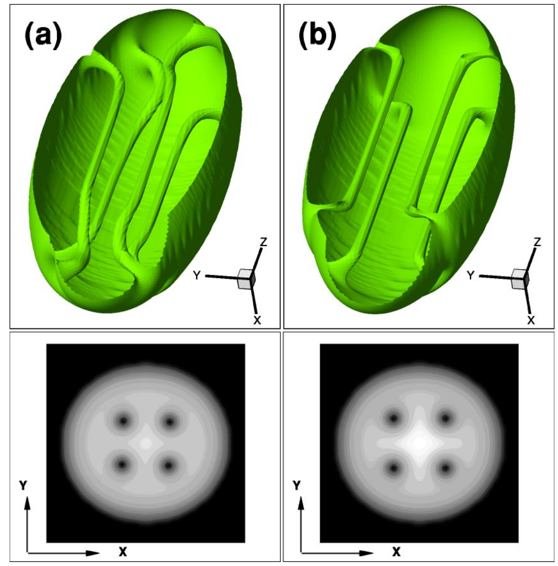

FIG. 13. Four-vortex configurations for (a) $\Omega/\omega_x = 0.86$—obtained from an initial condition without vortices and (b) $\Omega/\omega_x = 0.72$—obtained from an initial condition with four symmetrical vortices.

IV. CONCLUDING REMARKS

We have studied different vortex configurations in a prolate Bose-Einstein condensate by solving the Gross-Pitaevskii equation. We have computed *U* and *S* vortices, motivated by the recent experiments of Ref. [6]. Our computations involve a parameter ε, which is small when the number of atoms *N* is large. Decreasing ε, that is, increasing the number of atoms forces the vortex lines to be almost straight in their central part, while for larger ε, the central straight part is not so obvious as in some figures of Ref. [9].

We have found that the *S* vortices are only local minimizers of the energy and exist for all values of the angular velocity Ω, while *U* vortices are global minimizers existing for $\Omega \geqslant \Omega_c$. A planar *S* vortex can be regarded as a *U* vortex with a half part rotated by 180°. Moreover, *U* or planar *S* vortices lie only in the *x*-*z* or *y*-*z* plane while nonplanar *S* vortices exists only for an angle of 90° between the two branches.

We have followed the branches of solutions when varying Ω and found configurations with two, three, and four vortices.

[1] M.R. Matthews *et al.*, Phys. Rev. Lett. **83**, 2498 (1999).
[2] K.W. Madison, F. Chevy, W. Wohlleben, and J. Dalibard, Phys. Rev. Lett. **84**, 806 (2000).
[3] K.W. Madison, F. Chevy, W. Wohlleben, and J. Dalibard, J. Mod. Opt. **47**, 2715 (2000).
[4] C. Raman, J.R. Abo-Shaeer, J.M. Vogels, K. Xu, and W. Ketterle, Phys. Rev. Lett. **87**, 210402 (2001).
[5] J.R. Abo-Shaeer, C. Raman, J.M. Vogels, and W. Ketterle, Science **292**, 476 (2001).
[6] P. Rosenbusch, V. Bretin, and J. Dalibard, Phys. Rev. Lett. **89**, 200403 (2002).
[7] A. Aftalion and T. Riviere, Phys. Rev. A **64**, 043611 (2001).
[8] A. Aftalion and R.L. Jerrard, Phys. Rev. A **66**, 023611 (2002).
[9] J.J. García-Ripoll and V.M. Perez-García, Phys. Rev. A **63**, 041603(R) (2001); **64**, 053611 (2001).
[10] M. Modugno, L. Pricoupenko, and Y. Castin, e-print cond-mat/0203597.
[11] P. Orlandi, *Fluid Flow Phenomena* (Kluwer Academic, Dordrecht, 1999).
[12] S.K. Lele, J. Comput. Phys. **103**, 16 (1992).
[13] D. Butts and D. Rokhsar, Nature (London) **397**, 327 (1999).